ARTICLE

Selective Electroless Copper Deposition on Self-Assembled Dithiol Monolayers

Dmitry Aldakov,[†] Yvan Bonnassieux,[†] Bernard Geffroy,[‡] and Serge Palacin*,[§]

LPICM, and CEA LITEN, LPICM, Ecole Polytechnique, F-91128 Palaiseau, France, and CEA Saclay, DSM, IRAMIS, SPCSI, F-91191 Gif Sur Yvette, France

ABSTRACT The paper reports the use of self-assembled monolayers (SAMs) of dithiols to induce electroless copper deposition on a gold substrate. The metallization catalyst, palladium nanoparticles, is bound on the dithiol SAM. The assembly process is followed by IR and X-ray photoelectron spectroscopies to confirm the formation of a monolayer with bound catalyst. Electroless metallization is then carried out with a steady deposition rate of 130 nm/min. Additionally, microcontact printing of the catalyst on the SAM by poly(dimethylsiloxane) stamps is used to localize copper deposits. Resulting metallization is selective and allows for a high resolution.

KEYWORDS: electroless deposition • self-assembled monolayers • copper vias • dithiols • microcontact printing • palladium nanoparticles

INTRODUCTION

Electroless deposition of metals is of special interest in modern technology, especially in the fabrication of fine metal patterns for microelectronics, wear- and corrosion-resistant materials, medical applications, and battery technologies (1−5). Electroless deposition is based on the reduction of metallic ions from solution onto the substrate to be metalized without application of any electric current (6). This reaction generally requires the use of a catalyst that initiates the autocatalytic metallization process. The electroless process allows for selective and delicate metal deposition, which is often a challenge for electrolytic methods.

The crucial stage of the electroless deposition is seeding or catalyst deposition (also called activation). The catalyst particle lowers the activation energy of metal formation by serving as a temporary electron bridge between the reducing agent and metallic ions. After deposition of the first metal grains, the process becomes autocatalytic for many metals. The catalyst must be strongly bound to the substrate, and in the case of selective metallization, it should be localized strictly in the desired regions. Typical industrial surface activation processes involve surface treatment with stannous chloride followed by the reduction of Pd^{2+} to a catalytic form, colloidal Pd^0, by Sn ions adsorbed on the surface (7). Although widespread, that process involves the use of toxic tin compounds as well as numerous complex additives, surfactants, and other adsorption promoters. It lacks control over the size and morphology of colloidal palladium, which is known to determine the deposition behavior and deposit quality and does not allow selective deposition. Another approach of surface activation for electroless metallization is based on self-assembly methods. They can be applied for the metallization of a range of substrates by using different binding agents. These agents are typically bifunctional: one group anchors the agent to the substrate surface via the formation of a self-assembled monolayer (SAM), and the other allows for subsequent binding of the metallization catalyst. This approach has been thoroughly described for the metallization of Si/SiO_2 (2, 8−12). Some examples of SAM-based metallization of hydrogenated silicon (13) and plastic (14) substrates are also known.

Conversely, metallization of metallic substrates by such a surface activation method was much less studied because direct electrodeposition is generally more convenient in that case. However, in some cases an electric current cannot be applied directly to metallic substrates because of addressing problems, size limitations, or various geometric or material constraints. In those cases, electroless metal deposition (ElMD) becomes a vital alternative. To the best of our knowledge, only a few binding agents forming SAMs have been proposed for ElMD on metallic surfaces. For instance, mercaptocarboxylic acid based compounds allow catalyst-free metallization (15−17). While providing high-resolution patterns, this metallization process is very slow (6 nm/min), which limits its application only to thin patterns. Indeed, the probability of plating fog formation increases with time, which makes the plating bath unstable for high deposition rates (18). The alternative approach proposed by Delamarche et al. benefits from the high adhesion of the palladium catalyst to the surface of a titanium oxide coated substrate to exclude the use of SAMs (19). For that purpose, the authors had, however, to use unstable catalyst solutions and limit themselves to titanium substrates only. Application of functionalized polystyrene microbeads is an elegant but rather complicated way for selective nickel pattern deposition on polyelectrolyte film coated gold surfaces (20). Indeed,

* E-mail: serge.palacin@cea.fr.
Received for review October 22, 2008 and accepted January 19, 2009
[†] LPICM, Ecole Polytechnique.
[‡] CEA LITEN, LPICM, Ecole Polytechnique.
[§] CEA Saclay, DSM, IRAMIS, SPCSI.
DOI: 10.1021/am8001346
© 2009 American Chemical Society

Published on Web 02/11/2009

its resolution is limited by the size of the beads, and no information on the final conductivity of the deposits was given by the authors. Finally, it was recently shown that it is possible to metallize the gold surface using biphenylthiol cross-linkable SAMs (21). The metallization is rather slow (10 nm/min) and involves e-beam lithography for localization of the copper deposits. According to the authors, it provides only kinetic control over the deposition selectivity between cross-linked and pristine areas, which makes it problematic for use in electronic applications.

The present paper reports application of dithiol-based compounds as SAMs for binding noble metal nanoparticles aimed at catalyzing the electroless metallization process of metallic substrates. Thiol-functionalized molecules are known to form well-organized densely packed SAMs on the group 1b metals (22−24). They represent the best studied and widely used class of compounds for SAM formation. Also they are very promising materials for the fabrication of highly ordered and stable monolayers for chemical immobilization of nanoparticles onto metallic surfaces (25). For that latter purpose, the simplest strategy is to use dithiol molecules. Common dithiol molecules are commercially available and stable at ambient conditions. Provided that the chemical group that links the two thiol functions is rigid enough or short enough to prevent loop formation (26), they readily form a tightly bound well-organized monolayer on gold with a so-called "standing-up" phase (27) and provide molecular junctions with low resistance via electron tunnelling (28, 29). Dithiols have already been successfully employed to attach (25, 30, 31) or grow (32) semiconductor and metallic nanocrystals to metal surfaces.

In this work, we use 1,6-hexanedithiol (HDT) as a binding agent for palladium nanoparticle based catalyst immobilization onto gold surfaces. Subsequent copper electroless deposition provides a demonstration of the efficiency of the method that can be applied for the reliable, selective, and fast fabrication of metallic patterns for microelectronic devices.

RESULTS AND DISCUSSION

SAM Formation and Subsequent Catalyst Binding. The SAM formation process on gold was studied by IR reflection−absorption spectroscopy (IRRAS). On the IRRAS spectra (Figure 1), one can clearly see the aliphatic signature of the disordered hexyl chain (2856 and 2927 cm^{-1}) slightly shifted to lower wavenumbers with respect to ordered monolayers (25, 33, 34). As was already described in other dithiol SAMs including rigid ones that are not prone to loop formation, the SH stretch, which is typically present at 2600−2700 cm^{-1} for neat dithiols, is not discernible on the SAM spectrum. This lack of a S−H stretching signal is generally assigned to the poor signal-to-noise ratio of that specific group, or preferential orientation of the S−H bond for rigid dithiols (35). Upon binding of palladium nanoparticles on the HDT monolayer, the aliphatic peak becomes much more pronounced because of the added contribution of the capping ligands of the nanoparticles, namely, tetraoctadecylammonium chains.

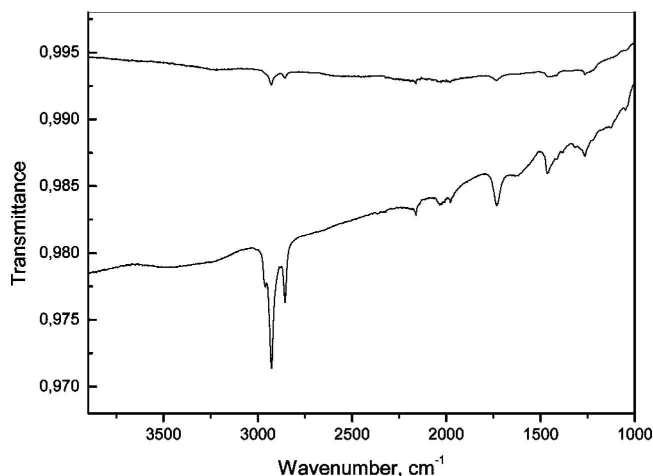

FIGURE 1. IR spectra of a HDT monolayer (top) and HDT with bound palladium particles (bottom). A vertical offset of 0.005 units for HDT/Pd was introduced for clarity.

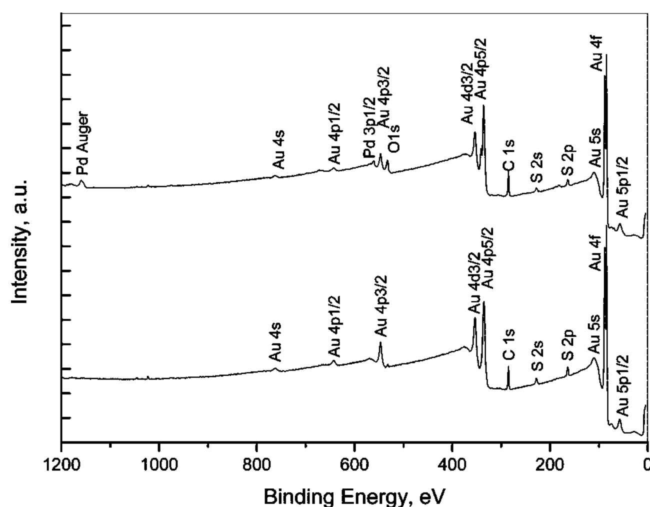

FIGURE 2. XPS spectra of a Au/HDT monolayer (bottom) and Au/HDT/Pd (top).

The contact angle measured on the resulting Au/HDT surfaces was 68°. This value is close to the previously reported contact angles for dithiol-based SAMs (28, 36) and confirms the formation of a monolayer on the gold surface. After the palladium nanoparticle binding, the hydrophobicity of the surface expectedly increases as witnessed by the contact angle of 90°, which confirms the successful adsorption of capped palladium nanoparticles.

In order to further investigate the palladium binding process on a HDT monolayer, we carried out a series of X-ray photoelectron spectroscopy (XPS) measurements. The survey XPS spectrum of a Au/HDT SAM reveals the presence of S atoms (Figure 2, bottom).

On the decomposed detailed spectrum (Figure 3, bottom), the sulfur peak appears as a superposition of two overlapping doublets of similar intensity: one at 162/163.5 eV and the other at 163.5/164.8 eV. They are attributed to (i) S bound to the gold surface (thiolate) for the former doublet and (ii) a "free" thiol group exposed to air for the latter one. X-ray diffraction and XPS measurements already demonstrated that diluted solutions of short-chain dithiol molecules predominantly take a "stand-on" conformation

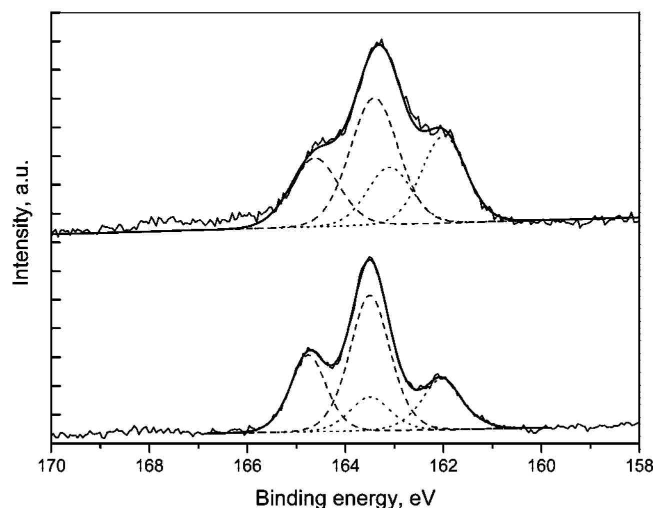

FIGURE 3. Sulfur XPS spectra of a Au/HDT monolayer (bottom) and Au/HDT/Pd (top). Fitted peaks of thiol and thiolate groups are represented by dashed and dotted lines, respectively.

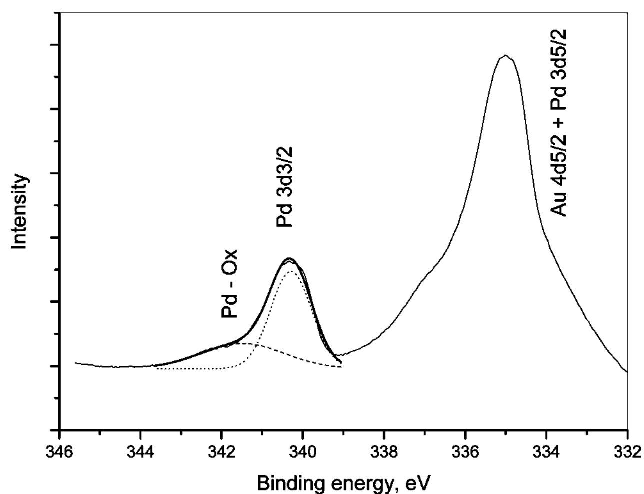

FIGURE 4. Pd XPS spectrum of Au/HDT/Pd (detail). Fitted peaks of Pd^0 and Pd-Ox are represented by dotted and dashed lines, respectively.

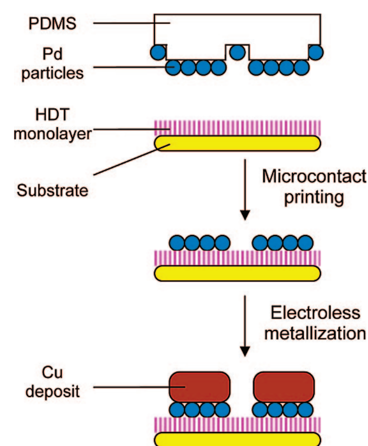

FIGURE 5. Scheme of selective metallization.

rather than forming loops with bidentate coordination to the gold surface (27). Ideally, the S—H/S—Au intensity ratio should be unity. However, ratios going from 1:3 to more than 10 were reported in the literature. The lower ratios are generally attributed to dithiols partially forming loops with both S atoms bound to Au (32). The higher ones are explained by both the attenuation of the bound-S signal by the SAM itself and some multilayer formation. Our own spectra give a ratio of ca. 2.4, which may be interpreted using both of the above arguments (37, 38). Anyway, the XPS analysis confirms the availability of SH groups for subsequent palladium adsorption.

After palladium adsorption, the thiolate peak significantly gains in intensity at the expense of the thiol peak (Figure 3, top), which is clear evidence of the binding of formerly free thiol groups with palladium nanoparticles. One cannot, nevertheless, rule out a possible migration of some unbound HDT chains trapped within the SAM and their binding on top of the palladium nanoparticles, which would result in a similar spectrum. Unfortunately, S atoms bound to Pd cannot be distinguished from S atoms bound to Au on the XPS spectra.

Palladium nanoparticle deposition onto the HDT monolayer should also be evidenced by the appearance of characteristic palladium peaks in a survey XPS spectrum. Unfortunately, most of the internal electronic transitions of Pd atoms show energies similar to those of Au atoms from the substrate, which prevents any accurate attribution. However, a weak 340.3 eV peak corresponding to Pd^0 $3d_{3/2}$ is visible on the detailed spectrum (Figure 4). Closer inspection of the palladium spectral region allows for detection of an additional peak at 341.5 eV. It can be attributed to an oxidized form of palladium (labeled as Pd-Ox in Figure 4), resulting from external oxidation or photoelectron bombardment, as was already observed for Pd $3d_{5/2}$ (39, 40). Finally, a clear Auger peak at 1160 eV (Figure 2, top) offers unambiguous evidence of the presence of palladium in the Au/HDT/Pd film.

Bulk Surface Metallization. Once deposition of the catalyst is realized, the surface is ready for electroless metallization. Electroless metallization was performed by using a copper plating bath with added triethanolamine (TEA), which was mixed with formaldehyde as a reducing agent (7). TEA actually adsorbs on copper surfaces in formation to inhibit formaldehyde oxidation, thus allowing for more control over the rate and quality of metallization (41). The substrate activated by a palladium catalyst was immersed directly into the plating bath for a given time, which resulted in uniform copper film growth on the Au/HDT/Pd surface. The copper film thickness is proportional to the metallization time. A metallization rate of 130 nm/min was measured by comparing the copper thicknesses on substrates metallized for various times. Its value remains constant for at least 5 min. The rate depends on the concentration of the reducing agent: the more formaldehyde, the faster the metallization, which results in films of lower quality. It should be noticed that the copper film quality, namely, morphology and surface roughness, is also often determined by the palladium activation process (42, 43). In our case, we found that the copper film properties were mainly influenced by the time of surface activation, i.e., the immersion time of the Au/HDT substrate in the palladium catalyst solution. Immersion of the substrate in the catalyst solution for a few seconds followed by metallization for 2

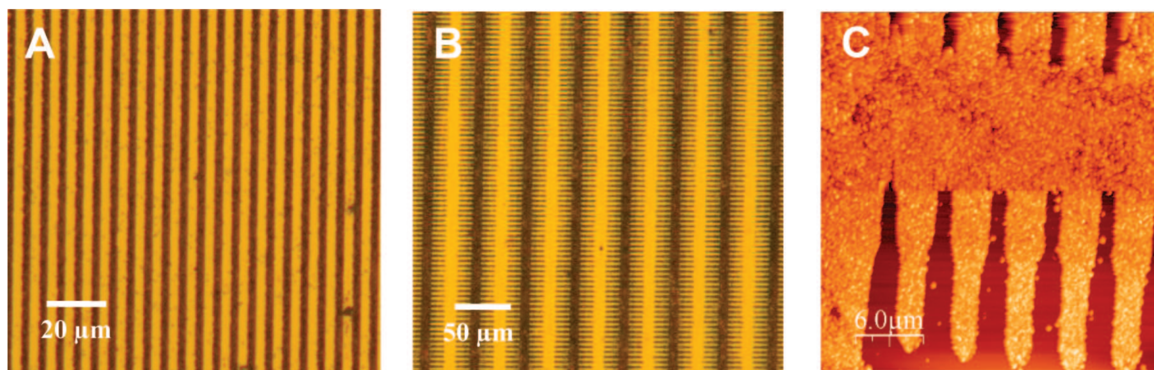

FIGURE 6. (A and B) Optical microscope images of gold substrates with different copper patterns deposited by microcontact printing. (C) AFM image of sample B.

min in a standard bath gave a final copper surface roughness of 33 nm, while treatment for 3 and 5 min resulted in R_{rms} values of 92 and 157 nm, respectively. Apparently, shorter exposure of Au/HDT SAMs to the colloidal palladium solution produces more homogeneous self-assembled Au/HDT/Pd layers, while an increase in the exposure time to the colloidal palladium solution leads to bulkier palladium aggregates, which results in rougher copper films.

Selective Surface Metallization. In order to carry out selective metallization of desired substrate zones, microcontact printing (44) was chosen to localize the palladium adsorption (Figure 5). The substrate surface was indeed patterned with catalyst particles by means of a poly(dimethylsiloxane) (PDMS) stamp, which was fabricated following standard procedures (45). Au/HDT substrates were prepared as described above. The patterned PDMS stamp was inked by the catalyst solution by dipping the stamp into a palladium nanoparticle solution in toluene, as described by Whitesides et al. (46). The stamp was then dried in an argon flow and brought in contact with the Au/HDT substrate for ca. 10 min. The pattern transfer occurred as a result of the spontaneous adsorption of palladium nanoparticles on available SH groups. The resulting patterned surface was then immediately immersed into the fresh copper plating bath followed by rinsing. Only the areas that were in contact with a stamp and thus contain a catalyst gave rise to copper deposition.

After metallization, the properties of the copper deposits were studied in detail. The deposits provide an excellent electrical contact between copper and the metallic substrate, with a resistivity approaching the values of copper and gold. That electrical continuity may arise from copper penetration through the catalyst and SAM layers to the Au/S interface. A similar phenomenon has been observed for catalyst-free electroless deposition on top of methyl- and carboxy-terminated thiols (17). Alternatively, that conductivity may be a consequence of efficient electron tunneling through the thiol layer (29, 47).

Depending on the stamp used, different patterns were obtained with high precision (Figure 6A–C). Small defects (isolated dots or incomplete coverage) in copper patterns are visible at high magnification. Contrary to Sawada et al., who showed direct copper reduction on top of SH-terminated monolayers (14), immersion of a catalyst-free Au/HDT surface directly into the plating bath did not give rise to any copper film formation within our typical experiment time (5–10 min). Hence, it is likely that the observed parasitic copper grains do not originate from defect sites in the HDT SAMs but are rather from experimental environment drawbacks such as working in an ordinary laboratory instead of a clean room. Similar defects are often observed following microcontact printing steps (45, 46). Nevertheless, the obtained micron-sized copper features are conformal to pristine PDMS stamps, which makes this technique relevant for applications in large-area electronics (such as displays and radio-frequency identification tags).

Regardless of the activation method (i.e., either homogeneous from a solution or localized through stamping), copper deposits pass the "Scotch tape test", which evidences their high adhesion to the substrate surface due to strong binding between all of the components of the system. The copper film growth rate measured for localized ElMD was the same as that for plain surface metallization. However, the roughness analysis performed by atomic force microscopy (AFM) on a number of samples metallized under typical conditions gives a R_{rms} value of 60 nm for the patterns obtained by microcontact printing, which is almost 2 times higher than that on a homogeneous Au/HDT/Pd. This disparity likely comes from different pathways of copper nucleation. In the case of localized ElMD, some catalyst nanoparticle aggregation occurs on the surface of wetted stamps when toluene evaporates because of the nonspecific adsorption of palladium on PDMS. During subsequent metallization, those catalyst aggregates may affect the surface morphology of copper deposits, including their roughness. In the case of homogeneous ElMD, the catalyst particles are firmly bound to the HDT SAM from a well-dispersed solution, which ensures better surface distribution and prevents aggregation during solvent drying. The resulting copper nucleation centers are smaller in size, hence the observed lower roughness.

This work demonstrates the successful application of bifunctional HDT as a monolayer on gold substrates for binding a palladium catalyst for electroless deposition of copper. HDT forms stable SAMs in a "standing-up" configuration, which provides a strong binding of palladium nanoparticles, as evidenced by IR spectroscopy and XPS. The

ARTICLE

catalyst can be deposited either by direct dipping of a substrate into the solution or by microcontact printing. The latter allows for the creation of finely patterned microstructures. Thin metal films grown on the activated substrates from a copper plating solution follow the defined catalyst pattern and exhibit high electrical continuity with the gold substrate. This simple and versatile method can be applied in microelectronics for the formation of conducting vias using only soft technologies, as well as in metal-coating modification.

EXPERIMENTAL SECTION

All of the reagents and solvents were used as received from the supplier without further purification. Glass substrates (RS France) were cleaned immediately before use by immersion in deionized water and placement into an ultrasonic bath for 15 min. The substrates were dried under an argon flow, and the procedure was repeated with ethanol and then acetone as solvents. Cleaned substrates were dried and subjected immediately to vacuum gold deposition. The gold thickness was 200 nm with the use of a sublayer of 20 nm of chromium as the adhesion promoter.

Surface Modification. Gold-coated slides were cleaned according to the procedure described above, followed by UV/ozone cleaning for 10 min right before the surface modification. The substrates were immersed into a 10 mM ethanolic solution of 1,6-hexanedithiol (HDT) overnight. Treated substrates (Au/HDT) were washed with fresh ethanol and dried under an argon flow.

For catalyst deposition, palladium nanoparticles stabilized with tetraoctadecylammonium bromide were synthesized according to the described procedure (46). The palladium nanoparticle diameter was ca. 5 nm with a narrow size distribution, as determined by transmission electron microscopy (see the Supporting Information). Au/HDT substrates were immersed into a 0.5 mg/mL solution of catalyst in anhydrous toluene for the desired time. At the end of palladium complexation, the Au/HDT/Pd substrates were washed with fresh toluene and dried under an argon flow.

Electroless Copper Plating. A typical copper plating bath was formed by mixing two solutions in a ratio of 6:1 right before the bath to be used. Solution 1: 2.9 g of $CuSO_4 \cdot 5H_2O$, 14.2 g of Rochelle salt, 4.2 g of NaOH, 2.5 g of Na_2CO_3, 1.7 g of ethylenediaminetetraacetic acid, and 0.43 g of triethanolamine in 100 mL of distilled water. Solution 2: saturated aqueous formaldehyde. The immersion time of the prepared substrates in the bath was on the order of 30−600 s and defined the resulting copper thickness. After the desired copper thickness was reached, the metal growth was stopped simply by rinsing the substrate with distilled water. All of the glassware in contact with metallization solutions was rinsed with nitric acid and distilled water.

Microcontact Printing of the Catalyst. PDMS stamps were prepared as reported previously (45) by using a Sylgard 184 kit from Dow Corning. Silicon wafers used as a master during the fabrication were treated in advance by (heptafluoroisopropoxypropyl)trichlorosilane vapor (Aldrich) to decrease PDMS adhesion to the silicon surface. Pattern transfer was performed according the procedure developed by Whitesides et al. (46).

Instrumentation. IR spectra were obtained with a Bruker Vertex 70 spectrometer (resolution 2 cm^{-1}; spectra were collected with 256 scans, MCT detector), equipped with a Pike Miracle plate for attenuated total reflectance. Contact-angle measurements were performed with water (Millipore) on a Krüss DSA 10 contact-angle measuring system, equipped with Krüss drop shape analysis software. XPS spectra were recorded on KRATOS AXIS ULTRA spectrometer with an Al Kα source monochromatized at 1486.6 eV. AFM measurements were performed on a Molecular Imaging PicoSPM AFM microscope (PicoScan 2100 controller, Scientec, France) under ambient conditions. Electrical conductivity of the deposited patterns was estimated using a two-probe Keithley 4200 system. Optical micrographs were obtained by a Leica DMLM microscope equipped with a Leica DFC320 digital camera.

Acknowledgment. The authors thank Pascale Jégou for XPS spectral measurements. The work was supported by ANR project ORGAPIX (ANR-05-BLAN-008-02).

Supporting Information Available: TEM micrographs of Pd nanoparticles and carbon and oxygen XPS spectra of Au/HDT and Au/HDT/Pd monolayers. This material is available free of charge via the Internet at http://pubs.acs.org.

REFERENCES AND NOTES

(1) Schlesinger, M.; Paunovic, M. *Modern Electroplating*, 4th ed.; Wiley: New York, 2000.
(2) Zabetakis, D.; Dressick, W. J. *ACS Appl. Mater. Interfaces* **2009**, in press (DOI: 10.1021/am800121d).
(3) Rao, C. R. K.; Trivedi, D. C. *Coord. Chem. Rev.* **2005**, *249*, 613–631.
(4) Michel, B.; Bernard, A.; Bietsch, A.; Delamarche, E.; Geissler, M.; Juncker, D.; Kind, H.; Renault, J.-P.; Rothuizen, H.; Schmid, H.; Schmidt-Winkel, P.; Stutz, R.; Wolf, H. *J. IBM Res. Dev.* **2001**, *45*, 697.
(5) Shacham-Diamand, Y.; Dubin, V.; Angyal, M. *Thin Solid Films* **1995**, *262*, 93–103.
(6) Brenner, A.; Riddell, G. E. *J. Res. Natl. Bur. Stand.* **1946**, *37*, 31–34.
(7) Lacourcelle, L. *Traité de galvanotechnique*; Galva-conseil: Millau, France, 1997.
(8) Ishida, M.; Kasuga, M.; Kaneko, T.; Shimoda, T. *Jpn. J. Appl. Phys.* **2000**, *39*, L227–L229.
(9) Zhu, P.; Masuda, Y.; Koumoto, K. *J. Mater. Chem.* **2004**, *14*, 976–981.
(10) Chen, M.-S.; Brandow, S. L.; Dulcey, C. S.; Dressick, W. J.; Taylor, G. N.; Bohland, J. F.; Georger, J. H., Jr.; Pavelchek, E. K.; Calvert, J. M. *J. Electrochem. Soc.* **1999**, *146*, 1421–1430.
(11) Dressick, W. J.; Dulcey, C. S.; Georger, J. H., Jr.; Calvert, J. M. *Chem. Mater.* **1993**, *5*, 148–150.
(12) Glickman, E.; Inberg, A.; Fishelson, N.; Shaham-Diamand, Y. *Microelectron. Eng.* **2007**, *84*, 2466–2470.
(13) Xu, D.; Kang, E. T.; Neoh, K. G.; Zhang, Y.; Tay, A. A. O.; Ang, S. S.; Lo, M. C. Y.; Vaidyanathan, K. *J. Phys. Chem. B* **2002**, *106*, 12508–12516.
(14) Sawada, S.; Masuda, Y.; Zhu, P.; Koumoto, K. *Langmuir* **2006**, *22*, 332–337.
(15) Zangmeister, C. D.; van Zee, R. D. *Langmuir* **2003**, *19*, 8065–8068.
(16) Garno, J. C.; Zangmeister, C. D.; Batteas, J. D. *Langmuir* **2007**, *23*, 7874–7879.
(17) Lu, P.; Walker, A. V. *Langmuir* **2007**, *23*, 12577–12582.
(18) Sugihara, S.; Iwasawa, A.; Onose, K.; Yamaki, J. *J. Appl. Electrochem.* **1996**, *26*, 63–71.
(19) Kind, H.; Geissler, M.; Schmid, M.; Michel, B.; Kern, K.; Delamarche, E. *Langmuir* **2000**, *16*, 6367–6373.
(20) Lee, I.; Hammond, P. T.; Rubner, M. F. *Chem. Mater.* **2003**, *15*, 4583–4589.
(21) Nottbohm, C. T.; Turchanin, A.; Gölzhäuser, A. *Z. Phys. Chem.* **2008**, *222*, 917–926.
(22) Ulman, A. *Chem. Rev.* **1996**, *96*, 1533–1554.
(23) de Boer, B.; Meng, H.; Perepichka, D. F.; Zheng, J.; Frank, M. M.; Chabal, Y. J.; Bao, Z. *Langmuir* **2003**, *19*, 4272–4284.
(24) Love, J. C.; Estroff, L. A.; Kriebel, J. K.; Nuzzo, R. G.; Whitesides, G. M. *Chem. Rev.* **2005**, *105*, 1103–1169.
(25) Nakanishi, T.; Ohtani, B.; Uosaki, K. *J. Phys. Chem. B* **1998**, *102*, 1571–1577.
(26) Bain, C. D.; Troughton, E. B.; Tao, Y. T.; Evall, J.; Whitesides, G. M.; Nuzzo, R. G. *J. Am. Chem. Soc.* **1989**, *111*, 321–335.

(27) Obeng, Y. S.; Laing, M. E.; Friedli, A. C.; Yang, H. C.; Wang, D.; Thulstrup, E. W.; Bard, A. J.; Michl, J. *J. Am. Chem. Soc.* **1992**, *114*, 9943–9952.
(28) Engelkes, V. B.; Beebe, J. M.; Frisbie, C. D. *J. Am. Chem. Soc.* **2004**, *126*, 14287–14296.
(29) Lindsay, S. M.; Ratner, M. A. *Adv. Mater.* **2007**, *19*, 23–31.
(30) Colvin, V. L.; Goldstein, A. N.; Alivisatos, A. P. *J. Am. Chem. Soc.* **1992**, *114*, 5221–5230.
(31) Ogawa, S.; Hu, K.; Fan, F.-R. F.; Bard, A. J. *J. Phys. Chem. B* **1997**, *101*, 5707–5711.
(32) Aliganga, A. K. A.; Duwez, A.-S.; Mittler, S. *Org. Electron.* **2006**, *7*, 337–350.
(33) Porter, M. D.; Bright, T. B.; Allara, D. L.; Chidsey, C. E. D. *J. Am. Chem. Soc.* **1987**, *109*, 3559–3568.
(34) Dubois, L. H.; Nuzzo, R. G. *Annu. Rev. Phys. Chem.* **1992**, *43*, 437–463.
(35) Colavita, P. E.; Miney, P. G.; Taylor, L.; Priore, R.; Pearson, D. L.; Ratliff, J.; Ma, S.; Ozturk, O.; Chen, D. A.; Myrick, M. L. *Langmuir* **2005**, *21*, 12268–12277.
(36) Henderson, J. J.; Feng, S.; Ferrence, G. M.; Bein, T.; Kubiak, C. P. *Inorg. Chim. Acta* **1996**, *242*, 115–124.
(37) Rieley, H.; Kendall, G. K.; Zemicael, F. W.; Smith, T. L.; Yang, S. *Langmuir* **1998**, *14*, 5147–5153.
(38) Rajalingam, K.; Strunskus, T.; Terfort, A.; Fischer, R. A.; Woll, C. *Langmuir* **2008**, *24*, 7986–7994.
(39) Gniewek, A.; Trzeciak, A. M.; Ziółkowski, J. J.; Kèpiñski, L.; Wrzyszcz, J.; Tylus, W. *J. Catal.* **2005**, *229*, 332–343.
(40) Xu, L.; Liao, J.; Huang, L.; Ou, D.; Guo, Z.; Zhang, H.; Ge, C.; Gu, N.; Liu, J. *Thin Solid Films* **2003**, *434*, 121–125.
(41) Lin, Y.-M.; Yen, S.-C. *Appl. Surf. Sci.* **2001**, *178*, 116–126.
(42) Patterson, J. C.; Ni Dheasuna, C.; Barrett, J.; Spalding, T. R.; O'Reilly, M.; Jiang, X.; Crean, G. M. *Appl. Surf. Sci.* **1995**, *91*, 124–128.
(43) Lau, P. P.; Wong, C. C.; Chan, L.; See, A.; Law, S. B. *J. Electrochem. Soc.* **2004**, *151*, C436–C438.
(44) Xia, Y.; Whitesides, G. *Angew. Chem., Int. Ed.* **1998**, *37*, 550–575.
(45) Kumar, A.; Biebuyck, H. A.; Whitesides, G. *Langmuir* **1994**, *10*, 1498–1511.
(46) Hidber, P. C.; Helbig, W.; Kim, E.; Whitesides, G. M. *Langmuir* **1996**, *12*, 1375–1380.
(47) Loo, Y.-L.; Lang, D. V.; Rogers, J. A.; Hsu, J. W. P. *Nano Lett.* **2003**, *3*, 913–917.

AM8001346